



*energies*



Article

---

# Optical Analysis of Ignition Sparks and Inflammation Using Background-Oriented Schlieren Technique

---

Moritz Grüninger, Olaf Toedter and Thomas Koch

Special Issue

Advances in Ignition Technology for Combustion Engines

Edited by

Prof. Dr. Vittorio Ravaglioli and Dr. Giacomo Silvagni



<https://doi.org/10.3390/en17061274>

## Article

# Optical Analysis of Ignition Sparks and Inflammation Using Background-Oriented Schlieren Technique

Moritz Grüninger <sup>\*</sup>, Olaf Toedter  and Thomas Koch 

Institute of Internal Combustion Engines (IFKM), Karlsruhe Institute of Technology, 76131 Karlsruhe, Germany

\* Correspondence: moritz.grueninger@kit.edu

**Abstract:** To determine the timing of inflammation in gas and gasoline combustion engines, the point of 10% mass fraction conversion of fuel (MFB10) is commonly used. The MFB10 can be determined from the heating curve, which in turn is calculated from the in-cylinder pressure curve. However, the cylinder pressure is an indirect parameter with regard to inflammation, as it is the result of the combustion that follows the inflammation. An attempt is made to derive a new, direct parameter of inflammation based on optical measurements in order to detect inflammation more rapidly and accurately. The background-oriented Schlieren technique (BOS) in combination with high-magnification optics and a high-speed camera is used to detect local density changes coming from the particle wave around the ignition kernel of a hydrogen combustion inside a combustion chamber. Via BOS and regular high-magnification high-speed imaging, the influence of ignition coil dwell time and in-cylinder pressure on the spark phases and the inflammation itself are evaluated. As a potential direct parameter for inflammation, the size of the particle wave resulting from the expanding ignition kernel is evaluated. It was found that a higher coil energy supports a faster propagation of the particle wave at ambient pressure. At higher pressures, general combustion effects override the effect of the influence of the coil energy on the propagation speed of the particle wave. In addition, the presence of successful inflammation was found to influence the spark phases. A directly measurable parameter for ignition could be found at a basic level, which will serve as a starting point for further detailed investigations.



**Citation:** Grüninger, M.; Toedter, O.; Koch, T. Optical Analysis of Ignition Sparks and Inflammation Using Background-Oriented Schlieren Technique. *Energies* **2024**, *17*, 1274. <https://doi.org/10.3390/en17061274>

Academic Editors: Giacomo Silvagni and Vittorio Ravaglioli

Received: 12 February 2024

Revised: 1 March 2024

Accepted: 5 March 2024

Published: 7 March 2024



**Copyright:** © 2024 by the authors. Licensee MDPI, Basel, Switzerland. This article is an open access article distributed under the terms and conditions of the Creative Commons Attribution (CC BY) license (<https://creativecommons.org/licenses/by/4.0/>).

**Keywords:** ignition; inflammation; optical analysis; BOS; background-oriented Schlieren; hydrogen; high speed; spark ignition

## 1. Introduction

For the evaluation of gasoline engine combustion processes, the inflammation timing in relation to the ignition spark timing, called burning delay, is crucial. Commonly used as inflammation timing is the point at which 10% of the fuel mass used is converted into heat (MFB10) and therefore pressure [1]. Heat losses are neglected in the calculation of MFB10. In some cases, other percentages such as 1 or 5% are also used, depending on the quality of the pressure curve. The MFB10 point can be calculated by using the in-cylinder pressure curve and deriving the summarized and then the normalized heat curve of it. The crank angle or point in time at which the normalized heat curve reaches 10% is the MFB10. Thus, the MFB10 is only an indirect parameter for inflammation, being deduced from global in-cylinder pressure, which in turn is the result of the combustion that follows the inflammation. To achieve faster and more secure recognition of inflammation, a new and direct measurable parameter is sought. We suggest using optical measurable parameters because of the high velocity of information transfer and locally high resolution. Optically it is either possible to use radiation from chemical reactions or, in this case, the presence of a local particle wave around the expanding ignition kernel. The particle wave that propagates around the ignition kernel and the subsequent flame kernel is locally close to and only dependent on the ignition kernel and is therefore a direct parameter for inflammation.

Because the particle wave is usually not visible to the human eye and cameras, we use an optical measurement technique called Schlieren. Schlieren allows changes in the local density over the optical path coming from particle waves, e.g., to be visualized. In the past, there have already been investigations using the classic Toepler–Schlieren method [2] to observe ignition sparks and inflammation. The Toepler–Schlieren technique requires a rather complex and precisely aligned optical path with collimated light and a knife edge. A few of the former investigations are the following: Shaffer et al. [3] investigated the ignition kernel during inflammation with the help of the Toepler–Schlieren method to better understand the plasma formation and propagation to assess the accuracy of their numerical modeling. Kozuka et al. [4] used a transparent cylinder engine to examine the effect of small deviations in the inflammation process on the cycle-to-cycle variations with the help of the Toepler–Schlieren method. They found that small differences in the initial combustion process are amplified by the movement of the piston and appear to be the reason for cycle-to-cycle deviations. However, the optical resolution of their setup is too low for our intended application. Essmann et al. [5] used high-resolution Toepler–Schlieren to measure the radii of particle waves following electrical discharges near the minimum ignition energy in dry air to investigate the effects of energy and energy density variations on the expansion of the kernel.

A modified version of the Toepler–Schlieren method called focusing Schlieren was also successfully used to observe initial flame kernel development and local quenching [6]. The focusing Schlieren method simplifies the measurement setup compared to Toepler–Schlieren, as collimated light and a single knife edge are not required. Instead of a knife edge, grids are used.

Since the superior goal is to be able to use the Schlieren measurement technique in a series combustion engine for inflammation detection without having to make major structural changes, we need a further simplification of the measurement technique. A fairly new version of Schlieren is background-oriented Schlieren. Its advantage is that it has a simple and robust design, allowing Schlieren images without special optical components by observing the shifting of a background pattern. BOS is not a direct imaging procedure, but requires post-calculation. It is described in Section 2. Potential vehicle integration requires further development in terms of the size and durability of the high-speed measurement technology. However, application in an internal combustion engine on a test bench is possible with today's measurement technology.

Using a high-speed camera and long-distance microscope, BOS is used in the spark gap of a spark plug in an optically accessible combustion chamber. With the same camera and experimental setup as for BOS, we are also able to capture highly magnified high-speed images of the ignition spark and its radicals and chemiluminescences simultaneously.

The aim of this paper is to show the suitability of BOS for inflammation analysis and to use BOS to analyze the influence of coil dwell time and in-cylinder pressure on the ignition spark phases and inflammation.

## 2. Materials and Methods

The experiments are carried out in a special optical combustion chamber of square base profile with planar optical accesses from front and back. The combustion chamber features hydrogen direct injection and automated charge cycle via electronically controlled valves. The optical accesses are designed to withstand 50 bar in-cylinder pressure. Ignition sparks are created by a standard automotive ignition coil with Iridium J-gap spark plug. The optical setup consists of a Phantom v2012 high-speed camera by Vision Research Inc., Wayne, NJ, USA coupled to an K2 DistaMax long-distance microscope by INFINITY PHOTO-OPTICAL GmbH, Göttingen, Germany and a green LED backlight (OSTAR Projection by ams-OSRAM, Premstaetten, Austria) behind the combustion chamber. A green backlight is chosen as it is in the range of the highest sensitivity of the CMOS sensor of the Phantom v2012. The COB (Chip-On-Board) LED is used with a lens set consisting of an optical diffuser, a collimator lens and a diffuser lens for more homogeneous illumination. The images

are captured with the software LaVision DaVis 10. Background-oriented Schlieren works like conventional Schlieren through the local change in the optical properties (refractive index) of gas when the density changes. This may occur because of pressure changes or other particle waves. BOS was introduced by Dalziel [7] (1998) and Meier [8] (2000). In contrast to conventional Toepler–Schlieren, however, BOS does not require perfectly parallelized back-lighting, carefully adjusted lenses and long optical paths resulting in a quite sensitive test setup [2]. For BOS, adequate illumination and a suiting, static background pattern are sufficient. It is, therefore, conceivable to use BOS in combustion engines with endoscopes. The background pattern should be placed directly behind the phenomenon under observation and contain randomly positioned dots in the size of estimated 3 pixels in camera resolution. The background pattern, consisting of a photo film with small dots, was mounted between two sapphire glass discs in a holder close behind the spark plug on the combustion chamber roof. As the refractive index between background pattern and camera changes, the background dots shift their position from the camera’s perspective resulting from the deflection of the light beams [9]. The displacement of the dots is then computed using reference images taken before the phenomenon. Hence, it is especially important for BOS that the background pattern is static, as any pixel shift leads to a recognized density change in post-processing. Each recorded sequence should contain around ten pictures before the phenomenon is observed. Finally, the local displacement of the dots and thus the locally resolved density change is displayed graphically in DaVis 10. The post-processed images are then exported for further image processing.

The experimental parameters are shown in Table 1. The whole test bench is automated via a National Instruments compactRIO (cRIO) module and a specially programmed control software (NI LabVIEW 2016). The data collection was realized via a cRIO AI module and a DEWETRON indication computer. The high-speed camera system is triggered by the cRIO system. Post processing of the pressure and temperature data was realized in Matlab R2020b.

**Table 1.** Experimental parameters.

Parameter	Value	Unit
Fuel	Hydrogen	-
Temperature	20	°C
Start Pressure	1 resp. 3	bar a
Lambda <sup>1</sup>	4.2	-
Ignition Coil Dwell Time	600 resp. 3600	µs
Framerate High-Speed Camera	75	kHz

<sup>1</sup> Lambda (air-fuel equivalency ratio) is the ratio of the actual AFR to the stoichiometric AFR for a given mixture.

For our research, we take high-speed images at two different combustion chamber starting pressures and different ignition coil dwell times. For further investigation, we also differ between ignition spark in air and ignition spark in air–fuel-mixture. All experiments were carried out for laminar flame propagation. Because of the high laminar burning speed of hydrogen [10], we had to increase lambda to decrease the flame speed to be able to depict the phenomenon adequately.

Optical post-processing in Matlab includes masking the electrodes, binarization and edge detection. After the binarization, only the largest contiguous spot is taken into account, assuming it is the particle wave. With this approach, it must be taken into consideration that inflammations and thus particle waves outside the largest spot could go unnoticed. However, since this is a laminar, knock-free combustion, we exclude inflammations outside the ignition kernel. The detected edge of the area is then marked graphically in color and outlined with a rectangle for comparison of the biggest two-dimensional outreach. In further research projects, advanced, intelligent image recognition and processing algorithms

based on machine learning could also be used to perform optical image post-processing and recognition, and to extract correlations from the images.

Information on the composition of the particle wave is important for a statement on the movement of the flame front of the combustion. Whether the particle wave is the result of the combustion reaction or the downstream gas propagation due to heating cannot be answered by BOS. BOS also cannot resolve whether the flame front moves in front of, in or directly behind the particle wave. Experiments that deal with the question of whether radicals that are formed by the ignition spark or combustion process (for example OH\*) move before or after the local density change are the subject of current research work and have not yet been completed. For this reason, we limit our statements to the fact that BOS makes local density changes visible and discuss a particle wave instead of a flame front. For better visualization of the influences on the spark phases (breakdown, arc phase and glow phase), we also take regular high-speed images in the visible spectral range (400–700 nm) of the sparks under the various test conditions. These images are not post processed.

### 3. Results

In this section, the selected results are presented and compared. For the comparison, certain representative time-steps of the experiments are chosen and shown side-to-side. The first time-step always contains the point in time when the breakdown happens. The time stamp is not correlated with the start of the electrical discharge and the ignition time, but with the camera recording start. Due to the reference images required for the BOS procedure, ten images are taken before the start of the electrical discharge.

#### 3.1. Influence of Dwell Time

First, the influence of the coil dwell time is analyzed. For this purpose, the coil dwell time is set to the minimal value and inflammation is just about possible in all considered operating points. This value is found to be 600  $\mu\text{s}$ . The other extreme regarded is a coil dwell time of 3600  $\mu\text{s}$ , at which the coil is in saturation. The experiments are carried out in the above introduced combustion chamber with the parameters presented.

##### 3.1.1. Without Fuel

As a reference for the other experiments, the influence of the dwell time was first examined in plain air. Figure 1 shows a timeline (from top to bottom) of the post-processed BOS images. The coil dwell time is 600  $\mu\text{s}$  on the left and 3600  $\mu\text{s}$  on the right side. The red line resembles the detected edge of the recognized area of the particle wave and, therefore, the local density changes. The rectangular box marks the largest two-dimensional extension of the recognized area. The electrodes are masked out in black. The gray-scale values indicate how much the background pattern is displaced compared to the reference image from the camera's point of view. The darker the values, the greater the displacement. In general, it can be said that the edge of the particle wave is well recognized. However, with small local density changes, as in this experiment, the contrast of the BOS images is low, which leads to a "frayed" edge of the detected area. The first row of images shows the point in time of the breakdown. A particle wave can be seen at both coil dwell times. The propagation of the particle wave differs slightly, that of the longer dwell time being slightly faster. In the following sequence, a faster propagating particle wave can be seen on the right-hand side. The two-dimensional shape of the particle wave is reminiscent of a lens shape with stronger lateral than longitudinal propagation. A spread around the cathode can also be seen here, possibly caused by a sliding base point of the plasma channel on the sides of the cathode and/or the plasma of the glow phase around the cathode. The three-dimensional propagation of the particle wave of an ignition spark could, regarding the gray-scale values, thus correspond to a shape such as a torus or biconcave disk. Comparing left and right, it can be clearly seen that the particle wave propagates faster and further when the coil is energized for longer.

The analysis of the high-speed images taken of the ignition spark shows the different spark phases. An ignition spark consists of three different phases at three different discharge mechanisms [11]. The first phase is the breakdown, which forms the initial discharge channel between the electrodes. The breakdown is a combination of the Townsend [12] and streamer mechanisms [13,14]. The electrons are accelerated in the strong electric field between the electrodes and generate free electrons and ions through collisions with particles. Further collisions result in an exponential increase in the number of free charge carriers. This is referred to as an avalanche or generation mechanism. If a certain number of free electrons in an avalanche is exceeded, a streamer can form. These streamers, in turn, are able to create an electrically conductive channel within a single avalanche [14,15]. The free electrons are, therefore, supplied by the impact ionization in the gas for this mechanism.

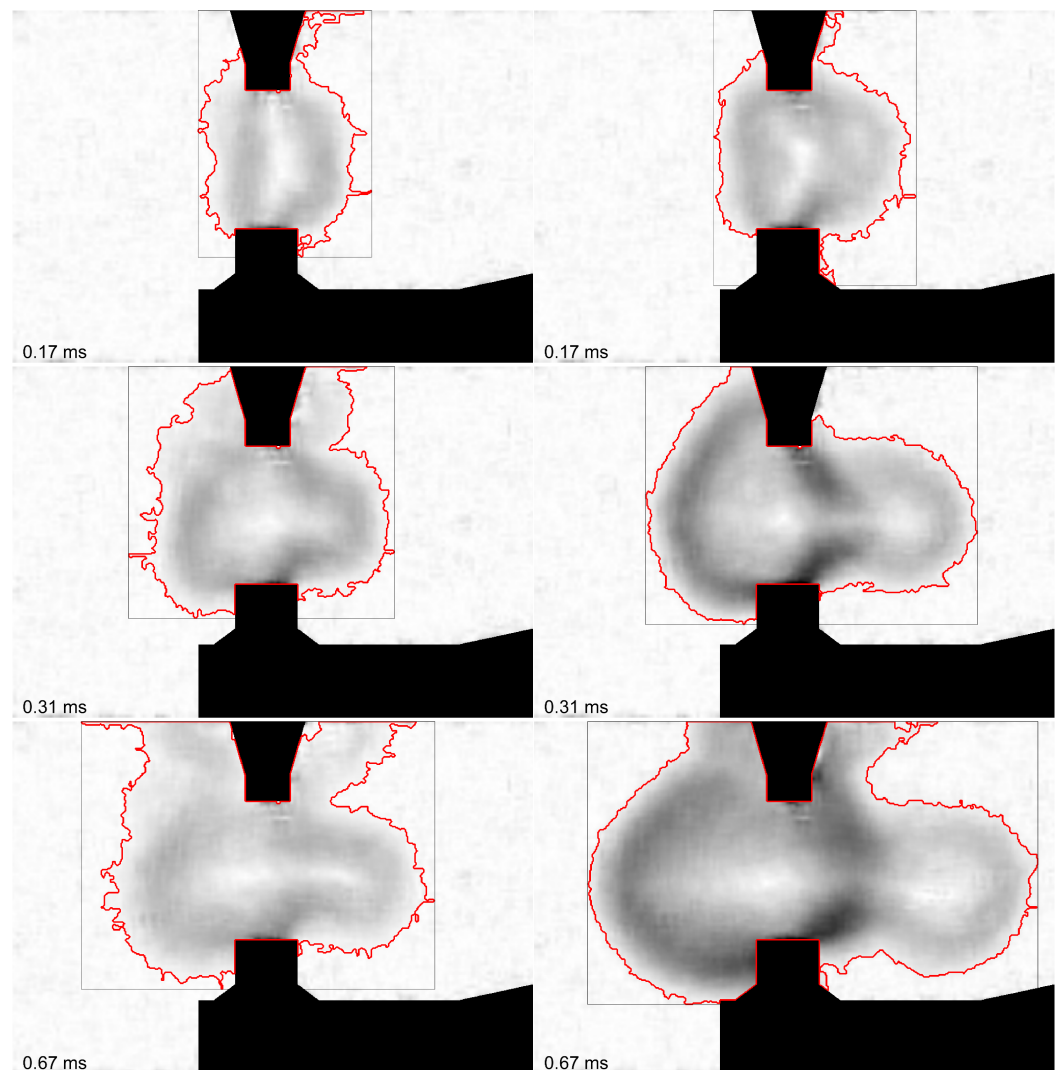


**Figure 1.** Background-oriented Schlieren (BOS) images. Comparison of dwell time at ambient pressure in air. Left 600  $\mu$ s, right 3600  $\mu$ s.

Following the breakdown are the arc phase and the glow phase, depending on the created plasma and the available discharged energy. The arc phase is characterized as a thermionic discharge [16]. During a thermionic discharge, electrons leave the cathode due to high temperatures and strong electric fields, forming a cathode spot. A thermionic discharge can provide high current densities [15,17,18]. This process is directly related to the wear of the cathode. The last and longest phase is the glow phase. Here, the electrons are provided by impact ionization in the gas, as with the Townsend discharge [15]. However, due to the lower field strengths, a glow film forms around the cathode instead of streamers.

The formed plasma between the electrodes consists of electrons, radicals, excited particles and ions [3,15].

Figure 2 displays a timeline (from top to bottom) of the high-speed images of two ignition sparks. The coil dwell time on the left is 600  $\mu\text{s}$  and on the right 3600  $\mu\text{s}$ . At the same pressure, the breakdown (top row) does not visually differ significantly with different available coil charging time and energy. However, it must be mentioned that optical differences in the breakdown are difficult to detect because the duration of a breakdown is an order of magnitude shorter than the exposure time of 13  $\mu\text{s}$ . As a result, it is likely that parts of the arc discharge can be seen in the first image, such as the base point on the anode (yellow due to excited eroded cathode material).

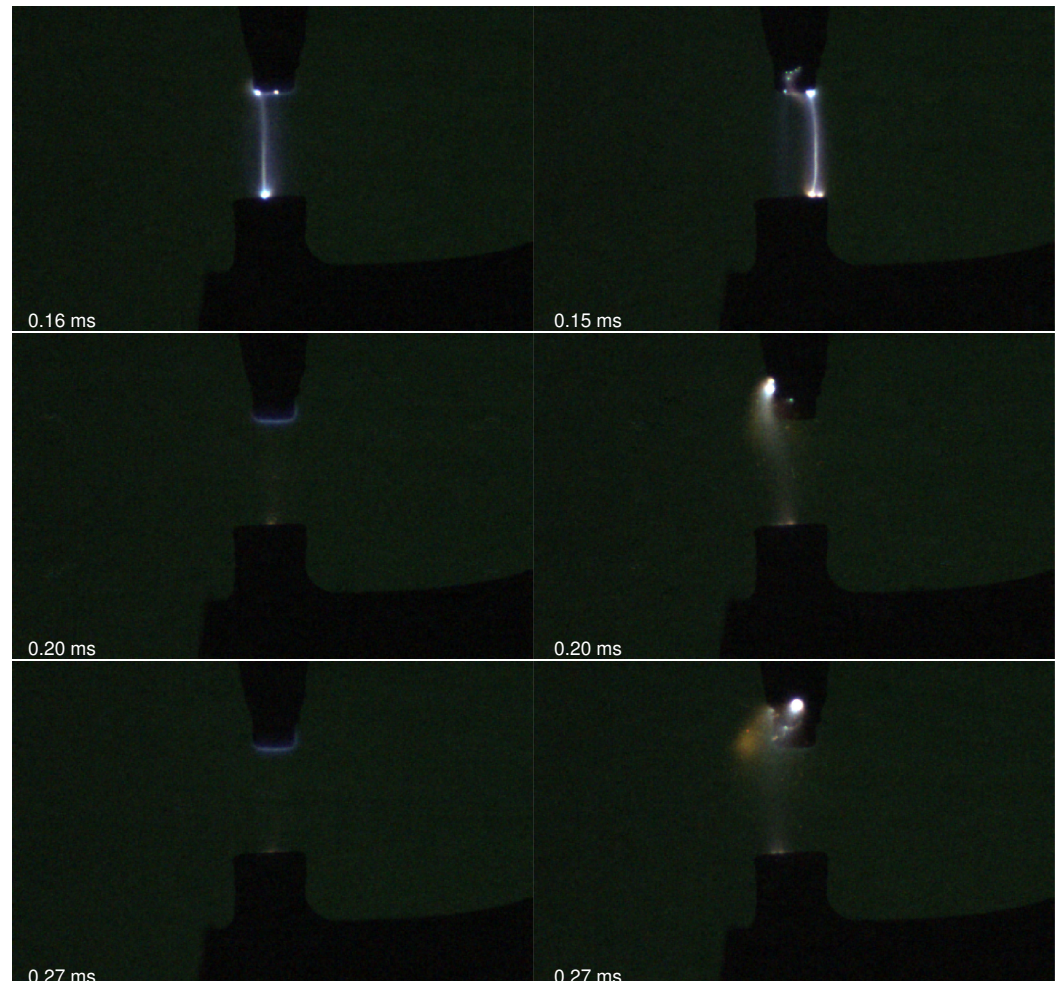


**Figure 2.** Comparison of dwell time at ambient pressure in air. Left 600  $\mu\text{s}$ , right 3600  $\mu\text{s}$ .

The duration of the spark phases after the breakdown differs significantly. In the right images, there is a clearly visible discharge channel. This visible discharge channel is formed by the arc discharge of the spark. Even at 0.27 ms, it is still distinctly recognizable. The upper base point of the channel skips on the cathode multiple times. Also, radiation of the excited vaporized cathode material is visible around the base point. The glow phase is recognizable by the blueish glow emission around the cathode and a small base point on the anode, as seen on the left side of Figure 2 (0.2 ms and 0.27 ms). For the shorter dwell time, there is no arc phase visible in the selected pictures.

### 3.1.2. With Fuel

In the previous section, the influence of the coil dwell time on the propagation of the particle waves at ambient pressure and in air was examined. This section will analyze the

influence of the dwell time on the propagation of the particle wave while combustion is starting. For this purpose, the combustion chamber is filled with a hydrogen–air mixture, which then is ignited by an ignition spark.

Figure 3 displays the timeline of post-processed BOS images of two inflammations with 600  $\mu\text{s}$  (left) and 3600  $\mu\text{s}$  (right) ignition coil dwell time. The first images (time-step 0.17 ms) show that the particle wave propagates slightly faster and with higher density gradients for longer coil dwell time. This phenomenon has already been observed without fuel. Compared to Figure 1, however, the propagation of the particle waves for short and long coil dwell time is nearly equivalent in the further course with a slightly faster propagation for longer coil dwell time. Moving pictures are provided in the Supplementary Materials of the online version of this article.

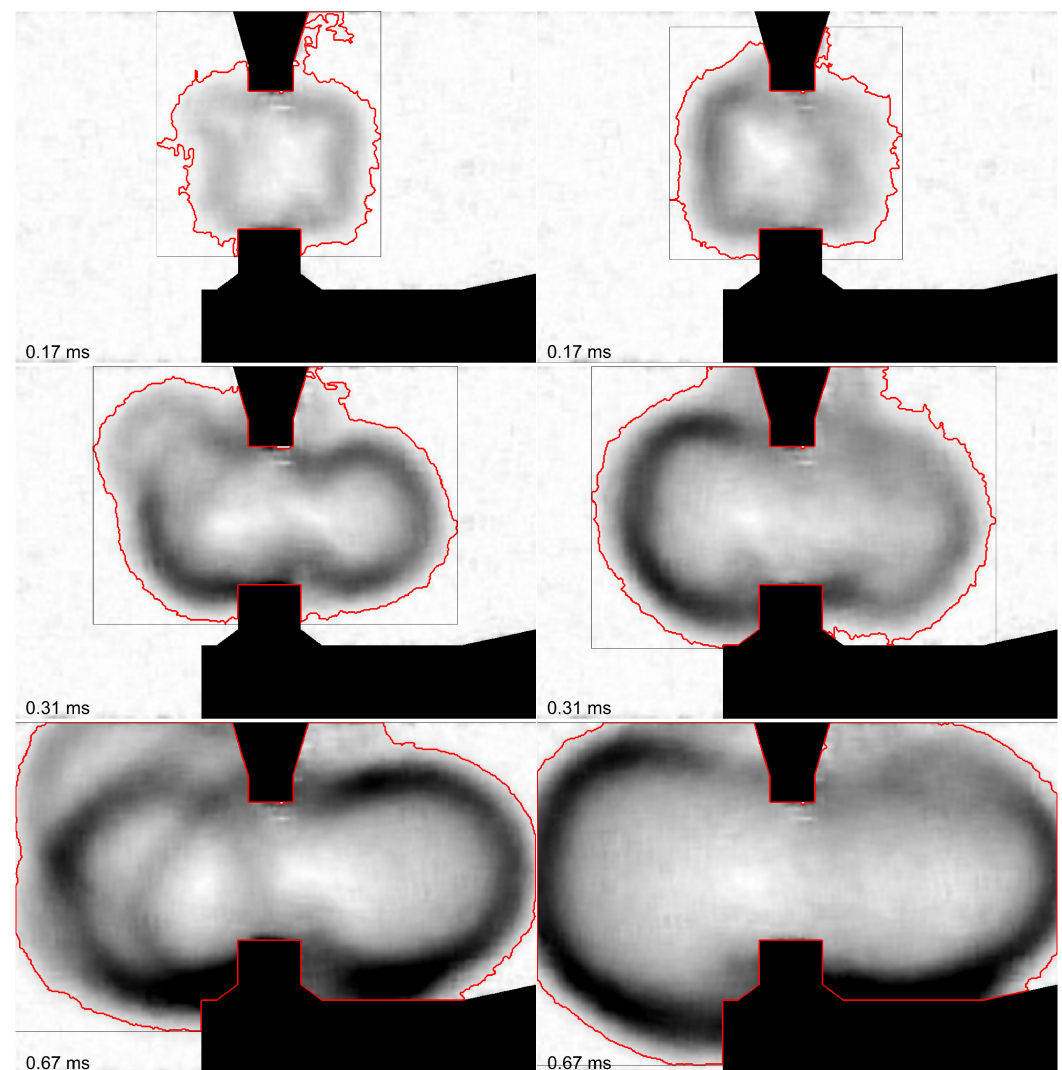


**Figure 3.** Background-oriented Schlieren (BOS) images. Comparison of dwell time at ambient pressure with hydrogen–air mixture. Left 600  $\mu\text{s}$ , right 3600  $\mu\text{s}$ .

The high-speed images of the ignition sparks in a hydrogen–air mixture in Figure 4 illustrate the effect of the plasma created by an ignition kernel on the ignition spark. The aforementioned brevity of the breakdown makes a precise assessment of the breakdown difficult. However, it appears that the light emission of the breakdown is weaker with an air–fuel mixture. Compared to a discharge in plain air (Figure 2 right), the arc discharge is massively shortened for a 3600  $\mu\text{s}$  dwell time. The discharge mode is already changing from arc to glow phase at the 0.2 ms time stamp picture. A distinctive feature here is that the light emission from the base point of the discharge channel on the anode and the

light emission from the glow around the cathode is much higher compared to the 600  $\mu$ s dwell time. This could be an abnormal glow discharge that occurs when the entire cathode surface is already involved in the discharge and the surface cannot be increased any further. In this case, the voltage is increased to ensure current transport [19]. The upper right image shows two base points of the discharge channel on the cathode, one of which is assumed to be afterglow. However, we can see that the base point of the discharge also moves here, but not to the sides of the cathode as in plain air (see Figure 2). For the short dwell time of 600  $\mu$ s, only a slight glow film around the cathode and, therefore, the glow phase is recognizable after the breakdown.

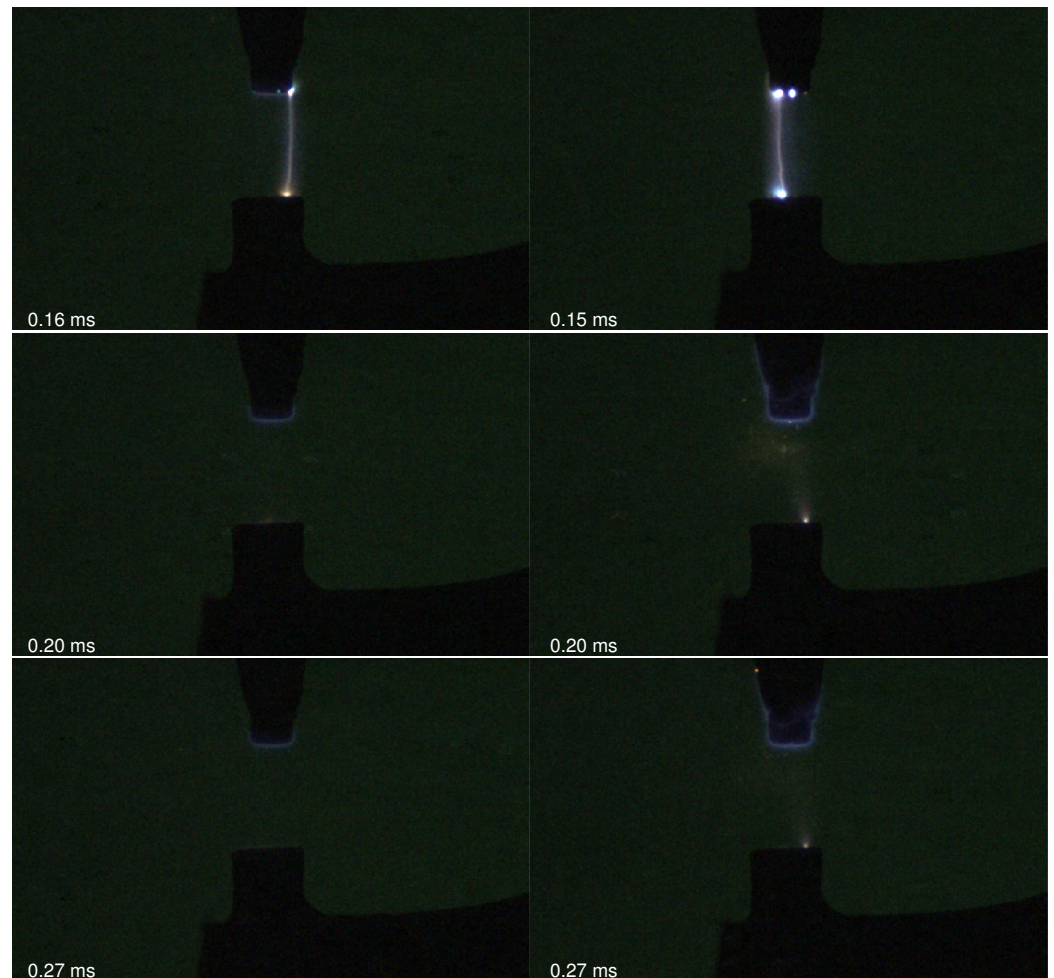


**Figure 4.** Comparison of dwell time at ambient pressure with hydrogen–air mixture. Left 600  $\mu$ s, right 3600  $\mu$ s.

### 3.2. Influence of Pressure

To analyze the influence of pressure on the expanding particle wave, further experiments are carried out in the constant volume combustion chamber. The combustion chamber is pressurized to higher pressures via an external compressed air supply. The difficulty at higher pressures is to get enough hydrogen into the combustion chamber for the desired  $\lambda$ , as it has a very low density. Significantly higher injection pressures are required for this purpose. As in the above shown experiments, a  $\lambda$  of 4.2 and a coil dwell time of 600  $\mu$ s is chosen. The short coil dwell time is intended to minimize the above-seen effect of an already-started inflammation on the spark phases and thus isolate the effects of the early stages of inflammation. The temperature in the combustion chamber is kept constant compared to the experiments at ambient pressure according to Table 1. Figure 5 depicts the BOS images of inflammations at 1 and 3 bar absolute pressure

at spark timing with a coil dwell time of 600  $\mu\text{s}$ . The first images (time-step 0.17 ms) show a difference in terms of the size of the particle wave. For the lower pressure, the particle wave is propagated further. Until this time stamp, only breakdown and possibly a short period of arc phase within the exposure time of the high-speed camera of about 13  $\mu\text{s}$  occurred. The images at the following time stamps (0.31 and 0.67 ms) show that the particle wave propagates faster at lower pressure, whereas at higher pressure, the gradients in density (darker gray-scale color) are bigger.

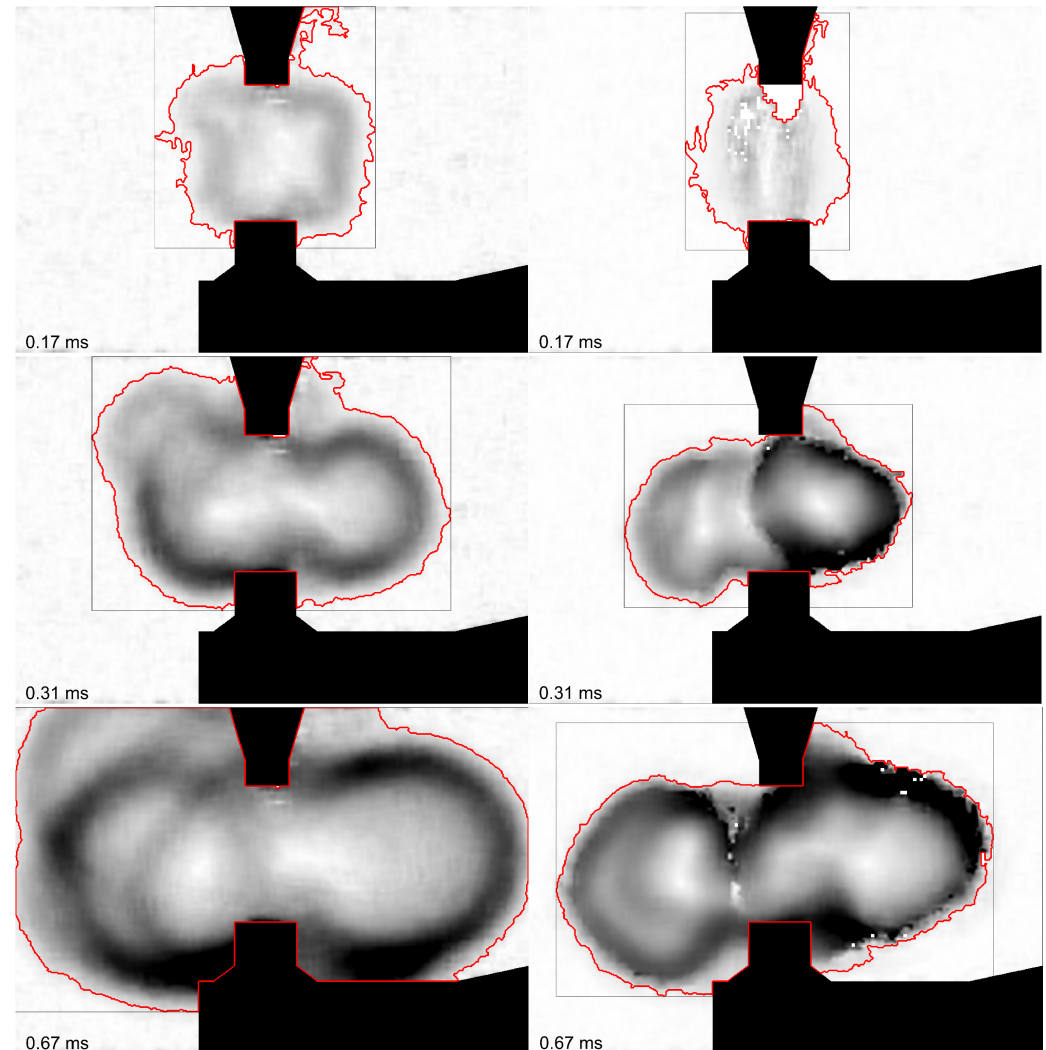


**Figure 5.** Background-oriented Schlieren (BOS) images. Comparison of different pressures with hydrogen–air mixture; 600  $\mu\text{s}$  dwell time. Left 1 bar, right 3 bar.

The analysis of the corresponding high-speed images (Figure 6) shows that the breakdown is significantly more light-intensive at higher pressure. The electrodes of the spark plug are illuminated due to the high light emission. Furthermore, discharge channels of an arc phase and a cathode spot (second time stamp) can be seen at a pressure of 3 bar. Here, two discharge channels are clearly visible between the cathode spot and the anode. Even at the third time stamp on the right, the cathode spot is still visible, which means that no change from arc to glow phase has yet taken place. In contrast, at 1 bar, only a thin glow film can be observed on the cathode after breakdown, which means that a glow discharge is present here.

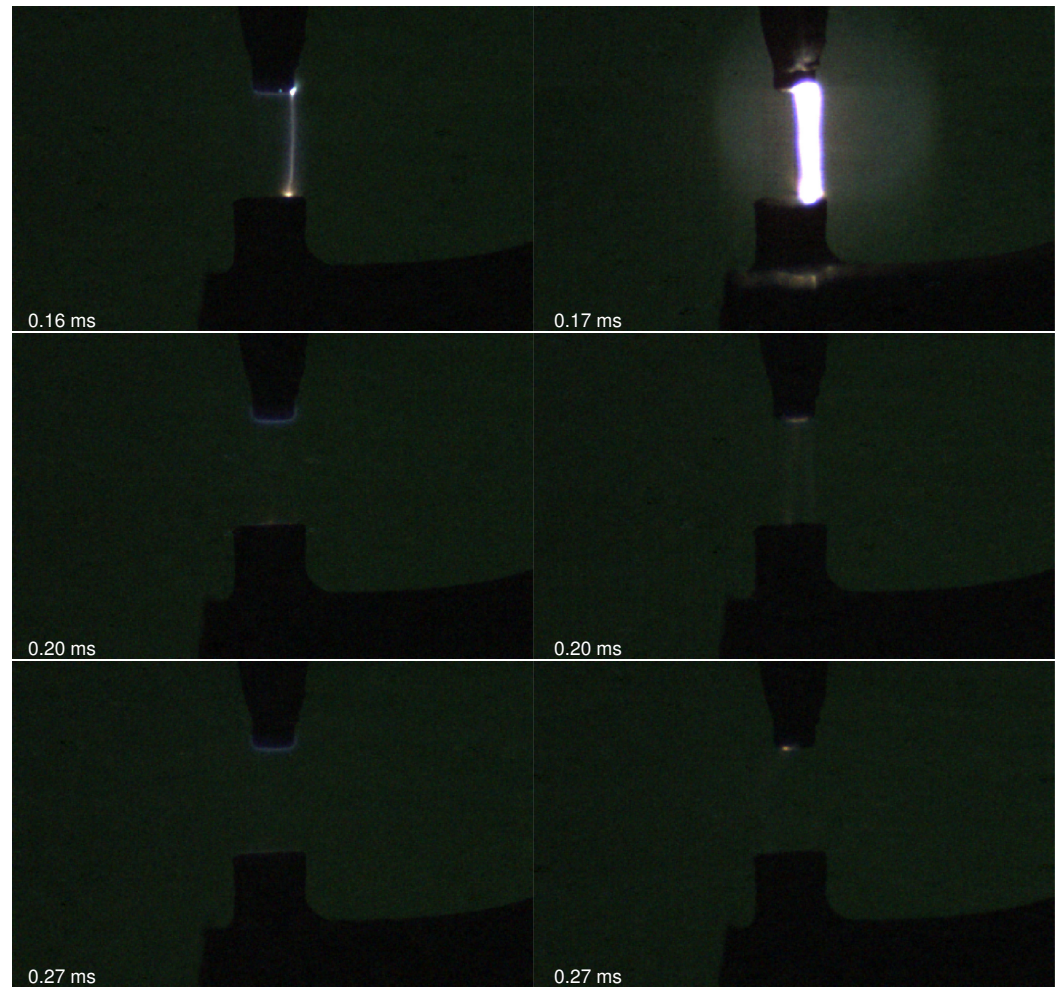


**Figure 6.** Comparison pressure with hydrogen–air mixture; 600  $\mu$ s dwell time. Left 1 bar, right 3 bar.

Figure 7 shows ignition sparks at 1 and 3 bar under the same conditions, only this time with a coil dwell time of 3600  $\mu$ s. Here, too, a higher light intensity of the breakdown can be seen at higher pressure. At 3 bar, a strong arc discharge forms, the base points of which do not skip on the cathode. Strong material erosion can be recognized by the light emission of the vaporized cathode material. Compared to ambient pressure, there is a change from glow discharge to arc discharge at higher pressures. This will be discussed in the following section and in [20].

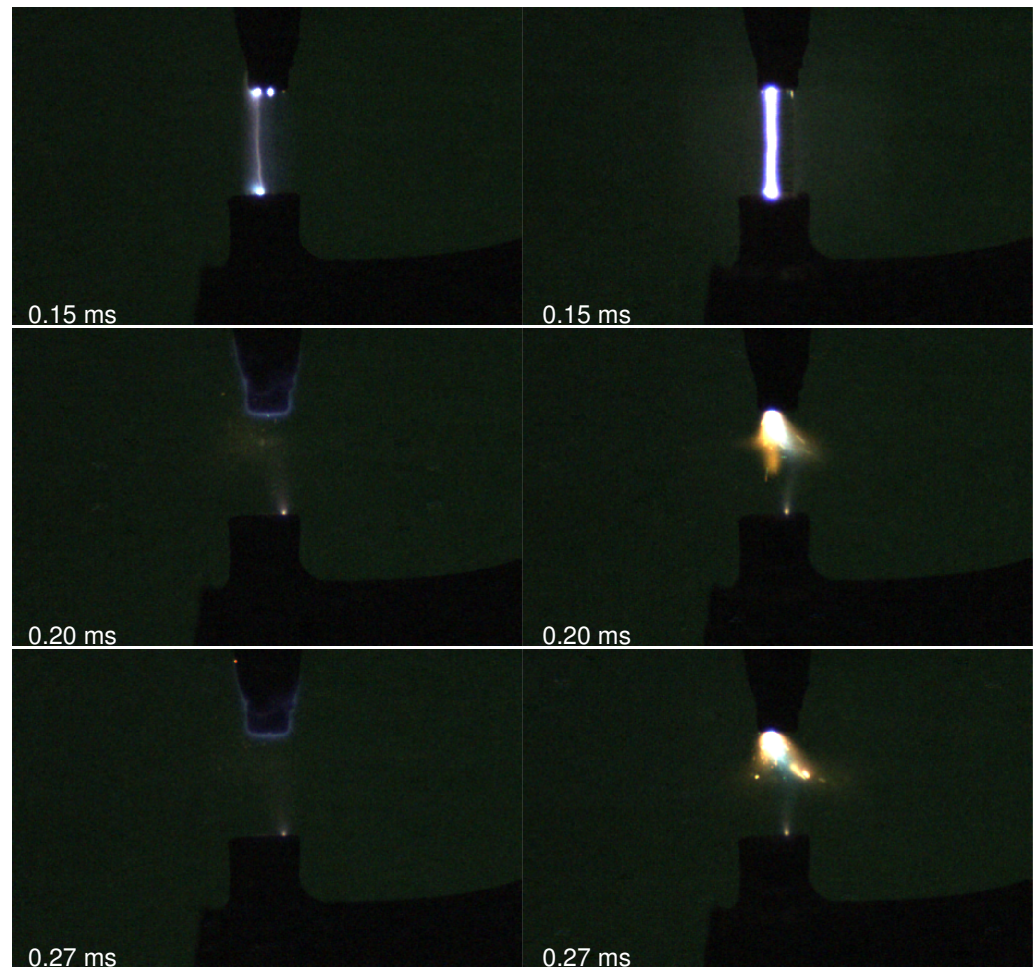


**Figure 7.** Comparison pressure with hydrogen–air mixture; 3600  $\mu$ s dwell time. Left 1 bar, right 3 bar.

#### 4. Discussion

This section will evaluate the results of the experiments against the theoretical background and place them in an overall context.

##### 4.1. Influence of Dwell Time—Without Fuel

The results of these experiments show a faster and further propagating particle wave for longer coil dwell time. The characteristics of the spark phases also differ for different coil dwell times. A longer dwell time results in a pronounced arc phase, while a short dwell time produces almost no arc phase, but almost exclusively glow phase after breakdown. The breakdown does not differ visually for different coil energies.

The stored energy in the coil follows

$$E = \frac{1}{2}LI^2 \quad (1)$$

with  $I$  being the current through the coil and  $L$  the inductance of the coil. The self-induction of the coil leads to a coil current characteristic during energization, as shown in Figure 8. The coil current in saturation depends on the ohmic coil resistance  $R$  and the applied voltage  $U_{Bat}$ . In our case, saturation is reached after approximately 3500  $\mu$ s. As a consequence of the longer dwell time, there is a higher current through the coil at the cut-off time. The higher current that is switched off abruptly induces a higher induced voltage, which leads to more stored energy in the parasitic capacitances on the secondary side of the ignition system. The secondary capacitances discharge partly in the breakdown and the remaining in the arc discharge, which can be maintained for longer with more available charge carriers.

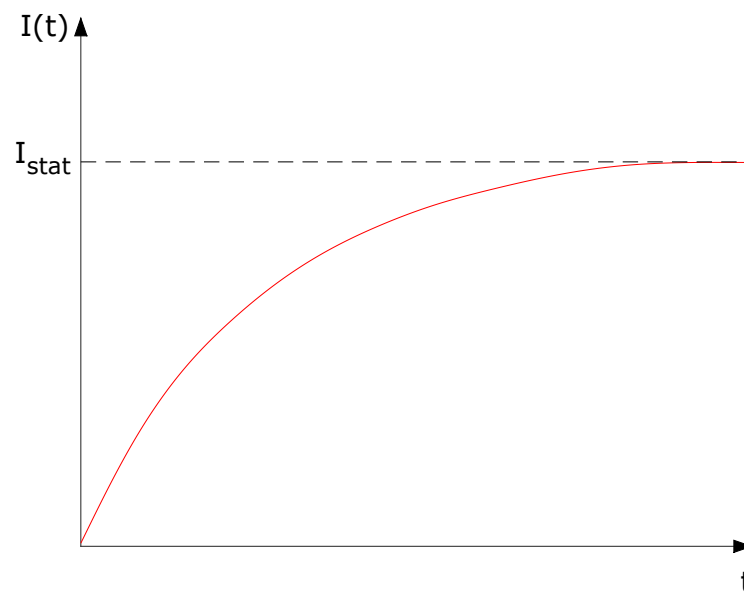


**Figure 8.** Current characteristic when energizing an ignition coil.

This experiment demonstrated the energy distribution over the spark phases. The energy that is needed for the breakdown stays the same, as the breakdown is mainly dependent on the pressure  $p$  and the distance between the electrodes  $d$ , which are kept constant here. This correlation was found by Paschen and described by Townsend 1915 [12]:

$$U_{Stat} = \frac{B \cdot pd}{\ln\left(\frac{A \cdot pd}{\ln(1 + \frac{1}{\gamma})}\right)} \quad (2)$$

$U_{Stat}$  corresponds to the static breakdown voltage,  $A$  and  $B$  being constants dependent on the gas type and reduced electrical field strength, and  $\gamma$  stands for the feedback coefficient. Due to the higher residual energy after breakdown with higher coil energizing, the arc phase is significantly stronger and longer. With an energizing time of 600  $\mu\text{s}$ , almost all the stored energy is needed for the breakdown, resulting in little to no arc phase. The remaining energy that could not be discharged in the arc phase because of a too-low current density is then discharged in the glow phase with a low current density.

Heat is released as a consequence of the collisions of particles in the electric field as well as the electric current flowing through the plasma channel (Joule heating) [17,21]. This heat causes expanding gas and therefore an expanding particle wave, which is detectable via BOS. This particle wave contains not only gas particles but also radicals created by electrical discharge and/or heat. So the bigger the amount of stored energy in the coil, the stronger and longer the arc phase (high current through plasma channel) and thus the higher the amount of heat released. Larger quantities of released heat generate larger and faster propagating particle waves. The breakdowns are identical for different coil dwell times at the same pressure according to the Paschen formula shown above and should therefore also release the same amount of heat and radicals. Since the exposure time of the BOS images in Figure 1 is about one order of magnitude longer than the duration of the breakdown, it can be assumed that the first image not only shows breakdown but also a small amount of arc phase. This explains the minimal greater expansion of the particle wave for a dwell time of 3600  $\mu\text{s}$  from the first time-step in Figure 1 because of more released heat.

#### 4.2. Influence of Dwell Time—With Fuel

When adding fuel to the combustion chamber, similar observations were made, but to a different extent. The particle wave has already spread slightly further in the first image

with a longer dwell time compared to a shorter dwell time. This phenomenon was already observed in Section 3.1.1. Compared to Figure 1, however, the propagation of the particle waves is significantly faster than without fuel, which means that a propagating ignition and flame kernel must have already formed in the first one-half of a millisecond after breakdown. Since the ignition spark and the forming ignition kernel are plasmas [3,17,18], it is possible to feed the ignition kernel with energy from the ignition spark. This leads to accelerated propagation of the ignition kernel. When chemical reactions are initiated on the surface of the ignition kernel, the latter becomes a flame kernel. If the flame kernel is big enough, it will become self sustaining, overcoming heat losses through quenching [3]. The crucial question is whether the flame kernel also acts as a plasma that will be fed and thus be further supported by the electrical discharge. Willems [22] states the flame kernel is no longer a plasma. Other researchers stipulate that a combustion flame is still a (weakly ionized) plasma [23–25] and could therefore also be fed through the ignition spark. Apart from this vagueness, it is difficult to separate the ignition core from the flame core, as the transition is seamless. The BOS images show that the propagation of the particle wave of higher coil energy discharge is slightly accelerated from the beginning of the electrical discharge as a result of a higher coil energy. This indicates that the forming flame kernel is supported by the electrical discharge, which backs the statement of [23–25].

The optical images of the ignition sparks in an air–fuel mixture show an additional special detail. If there is an air–fuel mixture between the electrodes, the discharge changes from an arc discharge to a glow discharge for otherwise identical test conditions (temperature, pressure, coil energy). The reason for this behavior must lie in the aforementioned properties of the formed flame kernel. The glow discharge is characterized by a constant current density, which is lower than in the arc phase [15]. If the discharge current is increased, the plasma area must increase as well to maintain the same current density. Due to an already formed flame kernel, the plasma area and volume between the electrodes is already increased. If the plasma area is large enough, the same current as in the arc phase can be transferred with lower current density in the glow phase. Thus, there are transitions between the arc phase and the glow phase. Combustion that has already started during the electrical discharge can therefore shorten the arc phase and cause a transition to the glow phase. This observation supports the statements of [23–25] in the form that either the flame kernel is a plasma or it must have plasma-like properties.

Maly established the theoretical relationship between the spark phases and the probability of inflammation [26] (see Figure 9).

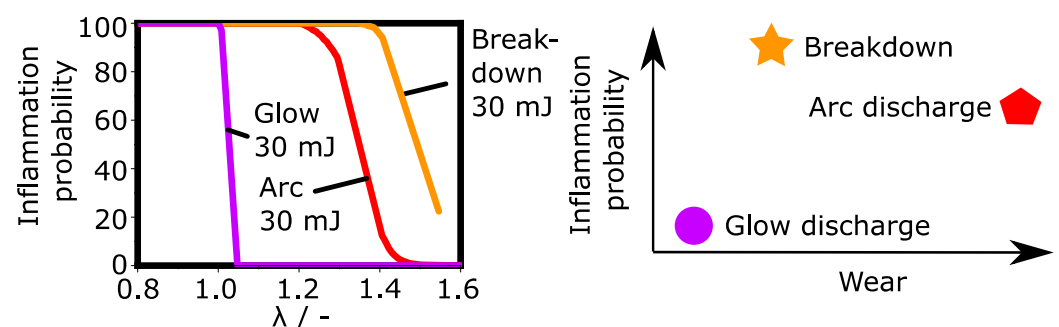


**Figure 9.** Inflammation probability versus lambda (left, for methane) and wear (right). Inspired by [26].

The breakdown shows the highest inflammation probability even for leaner mixtures with moderate wear as the electrons are supplied by the gas. The arc discharge shows good inflammability, but with high wear due to the physical processes of the thermionic discharge [26]. Characterized by low current density and electron supply by gas, the glow phase shows low inflammation probability but also low wear. However, as shown above, the glow phase can also feed an existing plasma and thus support inflammation over a longer period of time (milliseconds). In this context, it is particularly interesting to actually

see that the discharge mechanism changes with an existing flame kernel between the electrodes, resulting in a less abrasive process.

This experiment showed that a longer energizing time and thus a longer discharge time has advantages in the rapid propagation of the particle wave and the corresponding flame kernel. A prolonged discharge can be used to stabilize the inflammation at critical engine operating points. Furthermore, not only does the electrical discharge support the ignition kernel, but the presence of the ignition kernel also supports the plasma channel of the discharge.

#### 4.3. Influence of Pressure

The results of this experiment have shown that a higher pressure at the ignition timing does not lead to a faster propagation of the particle wave but to a far more light-intensive breakdown. In addition, the discharge channels of an arc discharge can be seen at higher pressure, in contrast to the experiment under the same boundary conditions at ambient pressure. According to Formula (2), higher pressure results in a higher static breakdown voltage. This means that as the pressure increases, more of the ignition coil's energy is shifted in the direction of breakdown. Higher energy, higher voltage and an increased particle density in the spark plug gap ensure a more light-intensive breakdown due to more excited particles emitting photons.

Previous published experiments in plain air have shown that the probability of arc discharge increases with higher pressure [20]. The higher amount of electrical charge carriers between the electrodes increases the probability for thermionic-field emission by a higher intensity of ion-bombardment on the cathode [27,28], resulting in increased cathode heating and therefore eased electron release. This observation can also be confirmed here. When the coil energy is also increased, a strong arc is created (see Figure 7). The slower propagation of the particle wave at higher pressure may be explained as follows. Since the breakdown at higher pressure needs more of the energy stored in the ignition coil, the available energy for arc or glow discharge is limited and therefore feeding of the ignition plasma is reduced. In addition, and mainly responsible for the slower propagation, thermo-diffusive instabilities of the flames with increasing pressure lead to a weaker and thus slower combustion process [29]. The observation shown above, that the arc discharge changes into a glow discharge in the presence of combustion, is therefore in competition with the increased probability of an arc discharge at higher pressures.

#### 4.4. Finding a Direct Parameter of Inflammation

Since ignition and combustion processes are described by many different reactions, including exponential ones, it is not easy to derive a direct parameter here. However, the already used particle wave is a projection of the reactions onto the two-dimensional, which we can measure directly optically. The simplest direct, optically measurable parameter is the detected area within the particle wave. In the case of the ignition spark without fuel, a reference sequence is recorded in which the maximum expansion of the particle wave is analyzed. This area can then be compared with that of inflammations in an air–fuel mixture. At the time-step, the area of the particle wave in the air–fuel mixture is larger than that of the reference spark in air, successful inflammation can be assumed. For this approach, the area on each image is evaluated from the binarized images and the progression of the area size is saved. However, the areas were only evaluated up to the point in time when they touched the edges of the image frame on the right, left or bottom. Unfortunately, it was not possible to position the electrodes differently in the image in this test setup due to parallel measurements for another purpose (not shown here). Due to the skipping base point of the discharge channel and the position of the cathode, the upper frame is often touched. If the images in which the particle wave touches the upper image frame are excluded, there are not enough images left for evaluation. The increase in area is significantly faster in the case of fuel and reaches the point at which the evaluation ended earlier.

The development of the area over time is then fitted to a second-order polynomial using curve fitting. The second order is chosen because, assuming a laminar flame speed, the volume within a perfect, spherical flame front or particle wave increases with  $r^3$ . Due to the two-dimensional camera observation, the area within the particle wave increases with  $r^2$ , with  $r$  being the radius of the kernel. It must be noted here that optimum observation is not possible with the existing experimental setup because of the aforementioned problem with image frame contact and the electrodes of the spark plug being in the image and thus distorting the detected area. The detected area is underestimated due to the areas of the masked electrodes and the areas that cross the image frame. This underestimation is not constant, but depends on the respective propagation of the particle wave.

At the beginning of the propagation, the entire surface is visible and is therefore correctly detected. As soon as the area overlaps the electrodes, the part that overlaps the masked area is not taken into account. The same happens if the surface crosses the frame of the image. The gradient of the area change curve will therefore be correct at the beginning of the analysis, but will underestimate the area in later phases, i.e., it will be too flat. The results of the tests at ambient pressure and 3600  $\mu\text{s}$  coil charging time are shown in Figure 10. It can be seen that the gradient of the area increase curve is significantly greater for the test with fuel and therefore the termination condition is reached earlier (approx. image 23). The curve is flatter for the test without fuel. Theoretically, a plateau should be reached, as the particle wave only propagates after the end of the discharge until the local temperature differences have equalized or the radicals/radical reactions no longer propagate due to a lack of energy supply or lack of combustion. For the experiment without fuel, the value of the fitted curve from the last evaluated time-step is taken and a horizontal line is drawn. The intersection of this line with the fitted curve of the experiment with fuel is taken and marked with a vertical line. The vertical line shows the time-step at which successful inflammation is assumed.

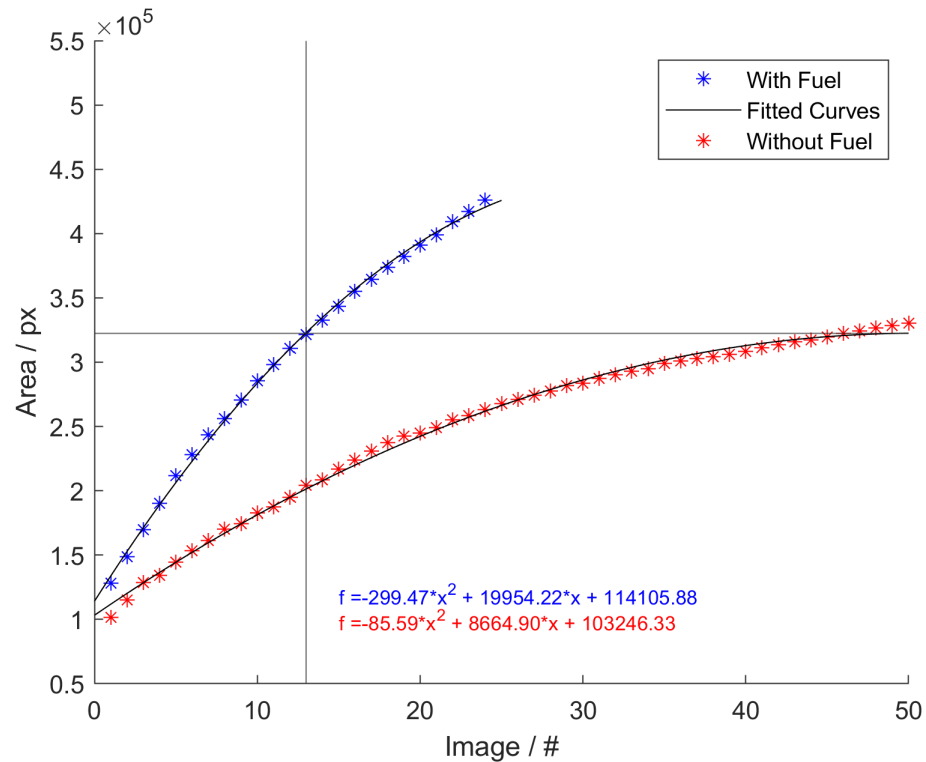


**Figure 10.** Comparison of particle wave area of ignition spark in plain air and in air–fuel mixture; 1 bar and 3600  $\mu\text{s}$  ignition coil dwell time. The grey lines mark the maximum area of the experiment without fuel and the point at which the experiment with fuel reaches the same area.

The MFB10 calculated from the pressure curve for this experiment is 55 ms, which correlates with image number 4125 at a frame rate of 75 kHz. An optical detection would recognize a successful inflammation at image number 13 (see intersection above).

The same evaluation method is applied to the experiments of 3 bar and 600  $\mu$ s ignition coil dwell time and shows the result shown in Figure 11. The calculated MFB10 for this experiment is 75 ms, which corresponds to image number 5625. As seen above, inflammation is detected much earlier optically.

To summarize, it can be said that the detection of inflammation via direct optical parameters works in a fundamental way. Inflammations are recognized much earlier compared to the method using the pressure curve. Further testing is needed to improve this method. The automatic detection of inflammations and the detection of flames that subsequently extinguish are also conceivable.

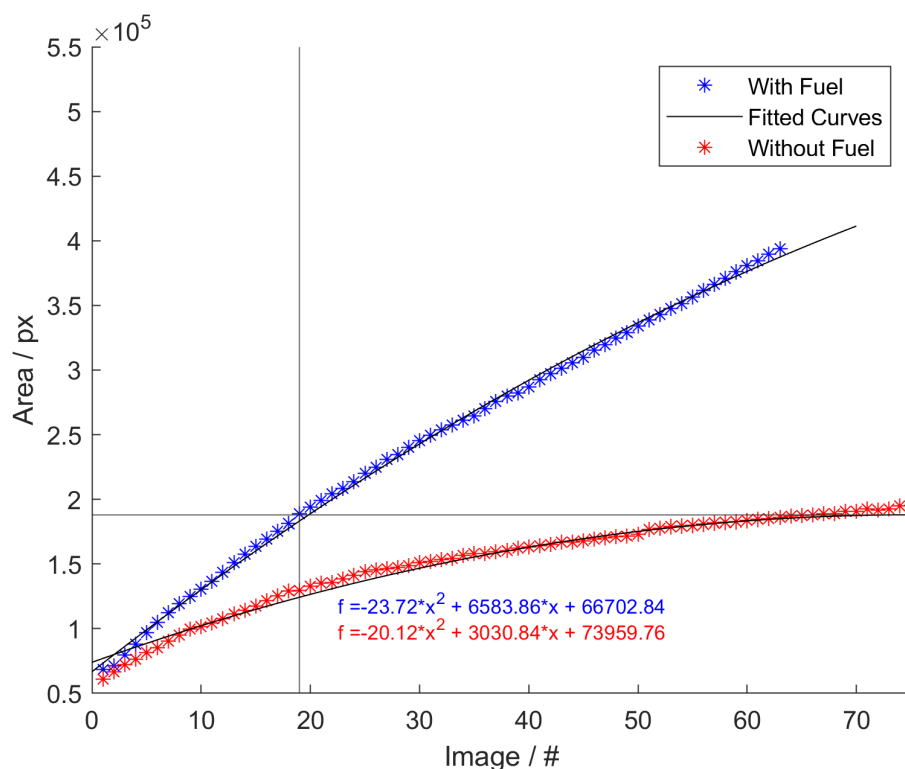


**Figure 11.** Comparison of particle wave area of ignition spark in plain air and in air–fuel mixture; 3 bar and 600  $\mu$ s ignition coil dwell time. The grey lines mark the maximum area of the experiment without fuel and the point at which the experiment with fuel reaches the same area.

## 5. Conclusions

Optical experiments were carried out to investigate the influence of ignition coil dwell time and combustion chamber pressure on the ignition spark and inflammation. It was shown that the BOS measurement method used is suitable for visualizing internal combustion engine inflammation. It was found that a longer coil dwell time leads to a faster propagation of the particle wave of inflammation at ambient pressure. Higher coil energy helps to enlarge the initial ignition kernel more rapidly due to a longer/stronger arc phase and plasma feeding. Higher pressure at the time of ignition leads to an increased probability of an arc phase and, due to the higher particle density, a larger number of excited particles. The propagation speed of the particle waves decreases with increasing pressure.

A direct optical parameter for ignition could only be found at a basic level. The size of the area of the particle wave from tests with fuel is compared with a reference area of a particle wave of an ignition spark in air. It has been shown that this method detects

inflammation much faster than the pressure-based method. However, this method is heavily dependent on optical parameters such as the field of view.

## 6. Outlook

It is the subject of ongoing research whether the chemical reaction of combustion takes place before, in or just after the particle wave. With this knowledge, the BOS images could be used directly to analyze flame fronts of combustions without the need for UV-capable measurement equipment.

**Supplementary Materials:** The following supporting information can be downloaded at: <https://www.mdpi.com/article/10.3390/en17061274/s1>.

**Author Contributions:** Conceptualization, M.G. and O.T.; methodology, M.G.; software, M.G.; validation, M.G. and O.T.; investigation, M.G.; data curation, M.G.; writing—original draft preparation, M.G.; writing—review and editing, T.K. and O.T.; visualization, M.G.; supervision, T.K.; project administration, M.G. and O.T. All authors have read and agreed to the published version of the manuscript.

**Funding:** This research received no external funding.

**Data Availability Statement:** The datasets presented in this article are not readily available because the data are part of an ongoing study. Requests to access the datasets should be directed to the corresponding author.

**Acknowledgments:** We acknowledge support by the KIT-Publication Fund of the Karlsruhe Institute of Technology.

**Conflicts of Interest:** The authors declare no conflicts of interest.

## Abbreviations

The following abbreviations are used in this manuscript:

AFR	Air–fuel ratio
BOS	Background-oriented Schlieren
CMOS	Complementary metal–oxide–semiconductor
COB	Chip-on-board
cRIO	Compact RIO (embedded Controller by NI Instruments)
LED	Light-emitting diode
MDPI	Multidisciplinary Digital Publishing Institute
MFB10	10% of mass fraction burned

## References

1. Heywood, J.B. *Internal Combustion Engine Fundamentals*; McGraw-Hill Inc.: New York, NY, USA, 1988; pp. 389–390.
2. Toepler, A. *Beobachtungen Nach Einer Neuen Optischen Methode*; Max Cohen & Sohn: Bonn, Germany, 1864.
3. Shaffer, J.; Luna, S.; Wang, W.; Egolfopoulos, F.N.; Askari, O. On the ignition kernel formation and propagation: An experimental and modeling approach. *J. Phys. D Appl. Phys.* **2023**, *56*, 225501. [[CrossRef](#)]
4. Kozuka, K.; Ozasa, T.; Fujikawa, T.; Saito, A. Schlieren Observation of Spark-Ignited Premixed Charge Combustion Phenomena Using a Transparent Collimating Cylinder Engine. *J. Eng. Gas Turbines Power* **2003**, *125*, 336–343. [[CrossRef](#)]
5. Essmann, S.; Markus, D.; Maas, U. Investigation of the Spark channel of Electrical Discharges Near the Minimum Ignition Energy. *Plasma Sci. Technol.* **2016**, *3*, 116–121. [[CrossRef](#)]
6. Ren, F.; Nakaya, S.; Tsue, M. Study on initial flame kernel development and local quenching effect during spark ignition process in a high-speed lean gasoline-air turbulent flow. In Proceedings of the International Meeting of Powertrains, Energy and Lubricants, Kyoto, Japan, 29 August–1 September 2023. [[CrossRef](#)]
7. Dalziel, S.B.; Hughes, G.O.; Sutherland, B.R. Synthetic Schlieren. In Proceedings of the 8th International Symposium on Flow Visualization, Sorrento, Italy, 1–4 September 1998; pp. 62.1–62.6.
8. Meier, G.E.A. Hintergrund Schlierenverfahren. Deutsche Patentanmeldung DE 19942856 A1, 16 July 2009.
9. Raffel, M. Background-oriented schlieren (BOS) techniques. *Exp. Fluids* **2015**, *57*, 60. [[CrossRef](#)]
10. Han, W.; Dai, P.; Gou, X.; Chen, Z. A review of laminar flame speeds of hydrogen and syngas measured from propagating spherical flames. *Appl. Energy Combust. Sci.* **2020**, *1–4*, 100008. [[CrossRef](#)]

11. Maly, R.; Herden, W.; Saggau, B.; Wagner, E.; Vogel, M.; Bauer, G.; Bloss, W.H. Die drei Phasen einer elektrischen Zündung und ihre Auswirkungen auf die Entflammungseinleitung. In Proceedings of the 5th Statusseminar Kraftfahrzeuge und Straßenverkehr, Bad Alexandersbad, Germany, 18 January 1977.
12. Townsend, J.S. *Electricity in Gases*; Clarendon Press: Oxford, UK, 1915; pp. 327–328.
13. Heintze, J. Elektrizitätsleitung im Vakuum und in Gasen. In *Lehrbuch zur Experimentalphysik Band 3: Elektrizität und Magnetismus*; Bock, P., Ed.; Springer: Berlin/Heidelberg, Germany, 2016; pp. 103–124.
14. Küchler, A. *Hochspannungstechnik: Grundlagen—Technologie—Anwendungen*, 3rd ed.; VDI-Buch; Springer: Berlin/Heidelberg, Germany, 2009. [[CrossRef](#)]
15. Michler, T. Ermittlung Charakteristischer Plasmaparameter der Funkenphasen von Zündfunken und Deren Bedeutung für die Entflammung. Ph.D.Thesis, Logos Verlag, Berlin, Germany, 2023.
16. Uhrlandt, D.; Baeva, M.; Pipa, A.V.; Kozakov, R.; Gött, G. Cathode Fall Voltage of Ac TIG Arcs from a Non-Equilibrium Arc Model. *Weld World* **2015**, *59*, 127–135. [[CrossRef](#)]
17. Fridman, A.; Kennedy, L.A. *Plasma Physics and Engineering*, 2nd ed.; CRC Press: Boca Raton, FL, USA, 2011.
18. Matveev, I.B.; Ardelyan, N.V.; Bychkov, V.L.; Bychkov, D.V.; Kosmachevskii, K.V. *Plasma Assisted Combustion, Gasification, and Pollution Control. Volume 1. Methods of Plasma Generation for PAC*, 1st ed.; Outskirts Press, Inc.: Denver, CO, USA, 2013.
19. Steenbeck, M. Zur Entstehung des normalen Kathodenfalles. *Z. Phys.* **1929**, *53*, 192–197. [[CrossRef](#)]
20. Grüninger, M.; Michler, T.; Lorenz, F.; Toedter, O.; Koch, T. Application of a time-resolved ignition spark measurement technique when using a power ignition system. In Proceedings of the 5th International Conference on Ignition Systems for Gasoline Engines, Berlin, Germany, 12–14 September 2022; pp. 81–96.
21. Wu, L. Kinetic Studies of Non-Equilibrium Plasma-Assisted Ignition and Combustion. Ph.D. Thesis, Drexel University, Philadelphia, PA, USA, 2013.
22. Willems, H.; Sierens, R. Modeling the Initial Growth of the Plasma and Flame Kernel in SI Engines. *ASME J. Eng. Gas Turbines Power* **2003**, *125*, 479–484. [[CrossRef](#)]
23. Lacoste, D.A. Flames with plasmas. *Proc. Combust. Inst.* **2023**, *39*, 5405–5428. [[CrossRef](#)]
24. Cancian, J.; Bennett, B.A.V.; Colket, M.B.; Smooke, M.D. Prediction of electron and ion concentrations in low-pressure premixed acetylene and ethylene flames. *Combust. Theory Model.* **2013**, *17*, 294–315. [[CrossRef](#)]
25. Uhm, H.S. Properties of plasmas generated by electrical breakdown in flames. *Phys. Plasmas* **1999**, *6*, 4366–4374. [[CrossRef](#)]
26. Maly, R. Spark Ignition: Its Physics and Effect on the Internal Combustion Engine. In *Fuel Economy: In Road Vehicles Powered by Spark Ignition Engines*; Springer: New York, NY, USA, 1984; pp. 91–148.
27. Rager, J. Funkenerosion an Zündkerzenelektroden. Ph.D. Thesis, Naturwissenschaftlich—Technische Fakultät, Herzogenrath, Germany, 2006.
28. Michler, T.; Kim, W.; Toedter, O.; Koch, T.; Bae, C. Influence of the Electrical Parameters of the Ignition System on the Phases of Spark Ignition. In Proceedings of the 4th International Conference on Ignition Systems for Gasoline Engines, Berlin, Germany, 6–7 December 2018; pp. 222–238.
29. Rieth, M.; Gruber, A.; Chen, J.H. The effect of pressure on lean premixed hydrogen-air flames. *Combust. Flame* **2023**, *250*, 112514. [[CrossRef](#)]

**Disclaimer/Publisher’s Note:** The statements, opinions and data contained in all publications are solely those of the individual author(s) and contributor(s) and not of MDPI and/or the editor(s). MDPI and/or the editor(s) disclaim responsibility for any injury to people or property resulting from any ideas, methods, instructions or products referred to in the content.